Received: 1 November 2019 | Revised: 6 March 2020 | Accepted: 16 April 2020

DOI: 10.1002/stc.2574

WILEY

RESEARCH ARTICLE

Improved long-span bridge modeling using data-driven identification of vehicle-induced vibrations

Etienne Cheynet[1,2] | **Nicolò Daniotti**[2] | **Jasna Bogunović Jakobsen**[2] | **Jónas Snæbjörnsson**[2,3]

[1]Geophysical Institute and Bergen Offshore Wind Center, University of Bergen, Bergen, Norway

[2]Department of Mechanical and Structural Engineering and Materials Science, University of Stavanger, Stavanger, Norway

[3]Department of Engineering, Reykjavík University, Reykjavík, Iceland

Correspondence
Etienne Cheynet, Geophysical Institute and Bergen Offshore Wind Center, University of Bergen, Bergen, Norway.
Email: etienne.cheynet@uib.no

Funding information
Norwegian Public Roads Administration

Summary

The paper introduces a procedure to automatically identify key vehicle characteristics from vibrations data collected on a suspension bridge. The primary goal is to apply a model of the dynamic displacement response of a long-span suspension bridge to traffic loading, suitable for automatic identification of the vehicle passage over the bridge. The second goal is to improve the estimation of the structural damping of the bridge deck by utilizing the free-decay displacement response induced by the passing vehicles. The vehicles responsible for a significant bridge vertical response are first identified using an outlier analysis and a clustering algorithm. Utilizing a moving mass model, the equivalent mass and speed of each vehicle, as well as its arrival time, are assessed in a least-squares sense. The computed vertical displacement response shows a remarkably good agreement with the full-scale data in terms of peak values and root-mean-square values of the displacement histories. The data acquired on the Lysefjord Bridge (Norway) indicate that the contribution of heavy traffic loading to the combined effects of wind and traffic excitation may be significant even at mean wind speeds above 10 m s^{-1}. The critical damping ratios of the most significant vibrational modes of the Lysefjord Bridge are studied for low wind velocities, using the time-decomposition technique and the traffic-induced free-decay response of the bridge deck. The structural damping ratios estimated this way are found to be more accurate than those obtained with an automated covariance-driven stochastic subspace identification algorithm applied to the same dataset.

KEYWORDS

ambient vibrations monitoring, full-scale measurements, long-span bridge, moving mass, traffic loading

1 | INTRODUCTION

The study of the interaction between vehicles and long-span bridges has been a popular topic since the 2000s. The term "vehicle–bridge interaction" refers here to modeling of both the bridge and the vehicle as a coupled dynamic system. In ambient vibrations monitoring, the term "traffic loading"[1] generally refers to a transient load induced by an undefined number of vehicles. Since the characteristics of these vehicles are unknown, the corresponding load is not modeled.

The study of vehicle–bridge interactions is a key research area for fatigue-life estimations,[2-4] by either modeling the load induced by traffic flow[5-7] or estimating the bridge modal parameters from the monitored vehicle-induced response.[8-14] The combined effects of wind and vehicle loading have also become an increasingly popular topic for, for example, fatigue analysis[15-17] or to assess the level of comfort and safety of passengers.[18-21]

One of the main purposes of ambient vibrations monitoring is to identify the structural modal parameters, namely, the eigenfrequencies, mode shapes, and damping ratios. In the case of a suspension bridge, the modal parameters are traditionally studied using a wind and structural health monitoring system (WASHMS), which combines vibration measurements and anemometer records. Atmospheric measurements are particularly valuable for evaluating environmental effects on the structural properties.[22,23] Algorithms dedicated to identifying modal parameters from ambient vibrations require generally a stationary excitation.[24,25] Even though traffic loading can be seen as a nonstationary source of excitation, it has commonly been used as input for modal identification with fairly good results.[1,26]

On the other hand, the combination of ambient vibrations monitoring and vehicle–bridge interaction is a topic rarely discussed, likely because identifying characteristics of moving vehicles using a WASHMS is challenging. The load applied by each vehicle is a function of the vehicle characteristics, which are a priori unknown. Similarly, vehicles arrive on the bridge at an unknown time and speed. In the case of a WASHMS without surveillance camera, additional sources of randomness are the number of vehicles moving simultaneously on the bridge as well as their direction.

The extraction of vehicle characteristics from the associated bridge vibration records has attracted attention for the past few years.[27-30] Unfortunately, these studies are limited to the case of a single crossing vehicle and short-span bridges. To the authors' knowledge, the automated identification of vehicle characteristics from long-span bridge vibration records is an unexplored topic. Yet the information collected this way is required to validate in full scale the modeling of the dynamic response of a long-span bridge to the passage of one or multiple vehicles.[31] Another key application of such identification algorithms is a more accurate estimation of the structural damping ratios, for the case of low wind speed conditions, when the vehicle-induced response is associated with a high signal-to-noise ratio. Finally, an algorithm of this type could be used to automatically identify whether long-span bridges in remote areas are regularly crossed by overweighted trucks. Such information can initiate detailed checking of structural integrity to avoid tragedies such as the one that occurred on the Pont de Mirepoix-sur-Tarn, in France, on November 18, 2019, due to the passage of an excessively heavy truck on the bridge.[32]

Traditional output-only identification techniques relying on ambient vibrations provide damping ratios estimated with a much higher level of uncertainty than the eigenfrequencies or mode shapes.[33,34] One of the main reasons is the sensitivity of the damping ratios on the mean wind speed and the record duration.[35-37] For a long-span bridge, the added aerodynamic damping can be larger than the structural damping. Therefore, the damping ratios of a wind-sensitive structure cannot be studied without simultaneous wind speed measurements.[38-40] The use of finite-duration ambient vibrations data leads to nonzero bias and dispersion that can be a major source of uncertainty. This is especially the case for the lowest modes of vibrations of long-span bridges.[36,38] Although longer record durations are desirable to reduce these uncertainties, stationary wind-induced response are seldom observed for a duration longer than 1 h. To circumvent these issues, the free-decay response of a long-span bridge induced by individual vehicles may be used instead of the entire response histories. This solution is particularly attractive as it does not require long-duration records and can be applied at low wind speed when the aerodynamic damping is negligible. However, it requires the identification of each vehicle crossing the bridge.

An automated algorithm able to identify vehicles crossing a long-span bridge is introduced in the following. This algorithm is suitable for modern long-span cable-suspended bridges in mountainous environments, such as those recently built in Norway or China, which have relatively little traffic due to theirrural location. Among the vehicle parameters studied, the arrival time and departure time of each vehicle are detected. When the wind loading can be neglected, these are used to establish the onset of the bridge free-decay response, from which the structural damping ratios of the structure are estimated. The proposed procedure complements traditional ambient vibration monitoring techniques by considering vibration records that are generally dismissed due to their highly nonstationary nature. In summary, the goal of the present study is twofold: first, we aim to automatically identify key characteristics of the

vehicles crossing a long-span bridge using a WASHMS and use them to model the vehicle–bridge interaction. Second, we aim to improve the estimates of the bridge damping ratios using the identified vehicle characteristics.

Section 2 describes the vehicle identification algorithm as well as the method applied to estimate the damping ratios and eigenfrequencies of a long-span bridge. Section 3 demonstrates the adequacy of the method to automatically estimate key vehicle characteristics using 1 year of full-scale vibration records from a long-span bridge in Norway. The influence of the wind loading on the bridge response compared to traffic loading is briefly discussed. Finally, Section 4 uses the detected vehicle arrival time and departure time to identify the vehicle-induced free-decay response of the bridge. It is shown that the damping ratios estimated this way often have lower dispersion and bias than those estimated using an automated stochastic subspace identification algorithm.

2 | METHODS AND DATASET

2.1 | The Lysefjord Bridge and its modeling

The structure studied is a long-span suspension bridge, named Lysefjord Bridge, located at the inlet of a narrow fjord in Norway. The bridge is surrounded by mountains and steep hills. It has a main span of 446 m and a 12.3-m-wide bridge deck with two traffic lanes and a walk path. At midspan, the bridge deck is 55 m above the surface. Although the traffic is on average low, it is also intermittent as the number of vehicles crossing the bridge are highly dependent on the schedules of a ferry, which lands only 2-km south of the bridge.

Since 2013, the Lysefjord Bridge has been instrumented with a wind and structural health monitoring system consisting of nine sonic anemometers and four pairs of three-axial accelerometers. In Figure 1, the position of the anemometers above the deck is defined using the hanger name H*XY*, where *X* is a digit between 08 and 24 indicating the hanger number and *Y* denotes the west side (W) or east side (E) of the deck. Since two anemometers are mounted on the hanger west no. 08 (H08W), the notations H08Wb and H08Wt refer, in the following, to the sonic anemometer mounted 6 m (bottom) and 10 m (top) above the deck, respectively. Eight of the sonic anemometers are 3-D WindMaster Pro from Gill Instruments (Lymington, UK), which can record the wind velocity and sonic temperature with a sampling frequency up to 32 Hz. The last sonic anemometer, mounted on H10W, is a Weather Transmitter WXT520 from Vaisala (Helsinki, Finland), which monitors the horizontal wind components, relative humidity, pressure, and absolute temperature with a sampling frequency up to 4 Hz. The accelerometers are CUSP-3D from Canterbury Seismic Instruments, which can operate with a sampling frequency up to 200 Hz. They are mounted inside the deck on each side of the girder to retrieve the horizontal, vertical, and torsional components of the bridge acceleration response. Five acquisition units are used to gather the data, which are synchronized and aggregated into a single file by a master data logging unit. Each file contains 10 min of record and is continuously transmitted via a mobile network. To facilitate data handling, the sampling frequency used for the analysis is set to 25 Hz. The Lysefjord Bridge is one of the rare suspension bridges in the world that has been studied by combining automated system identification techniques and meteorological measurements.[41] In this regard, the data collected are particularly valuable.

To describe the dynamic vibrations of the deck, the bridge is modeled using a continuum model,[42,43] to reduce the computational cost associated with the identification of the vehicles (Section 2.2). The modal parameters are computed using the Galerkin method and, if necessary, corrected using an operational modal analysis relying on an automated covariance-driven stochastic subspace identification (SSI-COV) algorithm.[40,44]

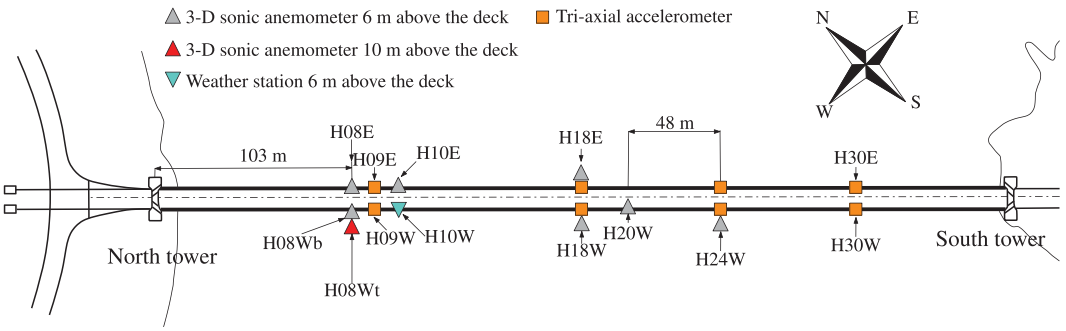

FIGURE 1 Instrumentation of the Lysefjord Bridge since July 2017

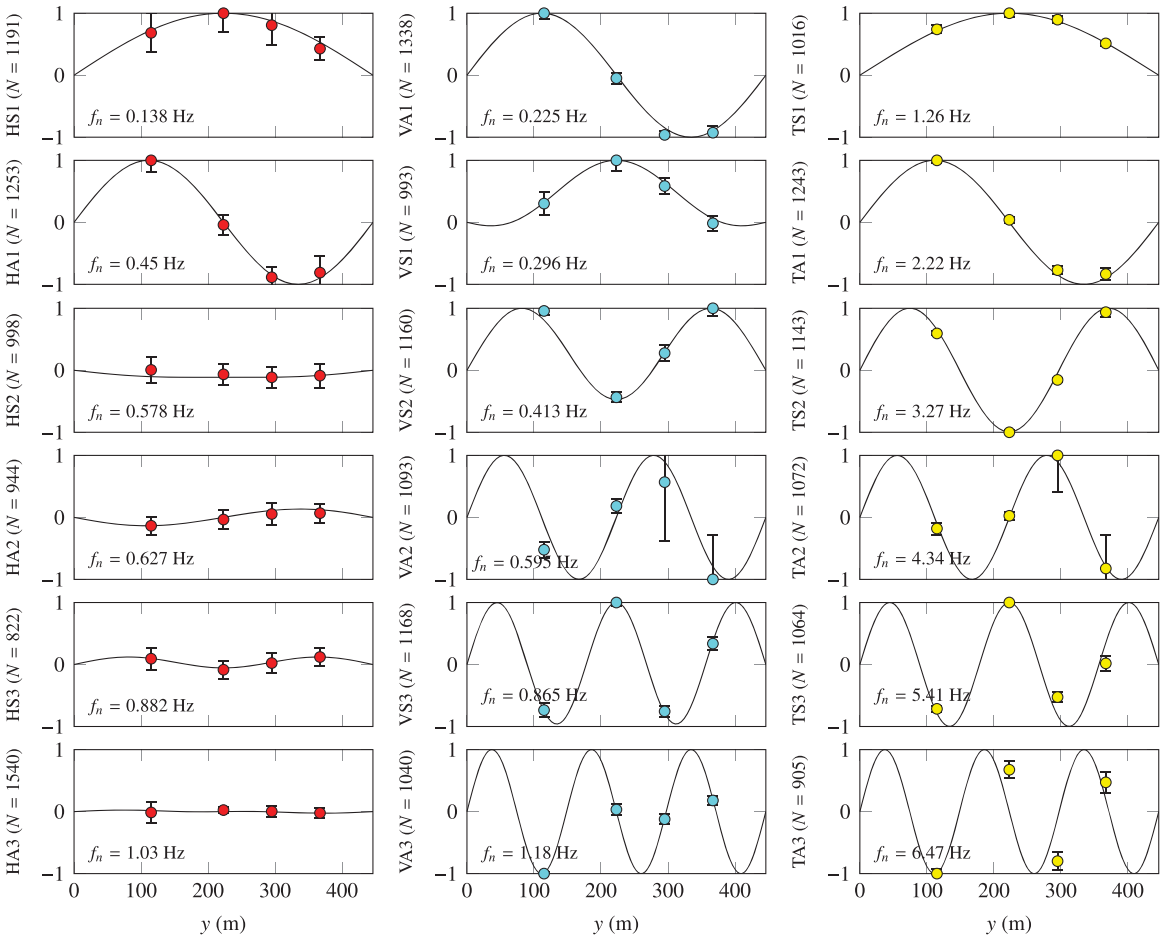

FIGURE 2 Computed (solid lines) and identified mode shapes (markers) of the Lysefjord Bridge deck in February 2018 with a mean wind speed below 5 m s^{-1} using the automated SSI-COV algorithm, where N is the total number of identified clusters per mode and the error bar corresponds to two standard deviations

Figure 2 superposes the first six computed lateral, vertical, and torsional mode shapes with those identified using the automated SSI-COV algorithm. As shown in Figure 2, each mode is identified using the string XYZ. The first letter $X = \{H,V,T\}$ represents the lateral (H), vertical (V), or torsional (T) degree of freedom. The second letter $Y = \{S,A\}$ is the symmetric (S) or asymmetric (A) feature of the mode shape. Finally, Z is a digit representing the mode number. The lateral mode shapes with a maximal value below unity are those for which the motion of the main cables is dominating over the deck motion. For the computation of the bridge deck response, the damping ratios are set equal to 0.2% for the modes VS1 and VS2 and 0.5% for the other modes, which is consistent with the expected damping ratio values of welded closed box girder.[45]

The initial motivation to instrument the Lysefjord Bridge with a WASHMS was to study its buffeting response,[46] including the torsional response of the bridge around its longitudinal axis. For this reason, pairs of accelerometers were installed inside the girder. Since the bridge main span has a width of 12.3 m for a length of 446 m, it was modeled as a line-like structure. The records from each pair of accelerometers were thus combined to compute the lateral, vertical, and torsional bridge acceleration response, at the four measurement locations. Figure 2 displays the prime components in the assumed uncoupled modes. Limited structural coupling between the horizontal and twisting components in the HS1 and TS1 modes, addressed in Wang et al., [47] is of secondary importance in the present work, which primarily exploits the vertical response data.

The mode shape corresponding to the mode VS2 (second vertical symmetric) was found to have a value close to 0 at midspan, even when using an alternative continuum bridge model by Luco and Turmo.[48] On the other hand, the identified mode shape had a value near 0.20, which was also predicted by a finite element model computed with the software ALVSAT.[49] To avoid a systematic underestimation of the computed bridge response at midspan, this particular mode shape was, therefore, corrected by the one computed with the finite element model. The computed and estimated mode

shape for the mode VA2 shows also some discrepancies. The uncertainties are in general much higher in the frequency range between 0.57 and 0.62 Hz due to the coupled motion of the bridge tower, main cables, and deck. The finite element model did not provide mode shapes that differed significantly from those computed with the continuum bridge model. As the mode VA2 has a limited influence on the bridge response at midspan, only the mode VS2 was corrected.

2.2 | Identification of vehicle characteristics from records at midspan

The study of vehicle–bridge dynamic interaction is generally conducted by describing each vehicle as a multiple degree-of-freedom system.[19,50-52] In that case, the accurate modeling of the high-frequency bridge response is crucial to provide realistic results. The situation described here is fundamentally different as vehicles are detected using the quasi-static vertical bridge response only, that is, the frequency range located below the first eigenfrequency. Besides, we focus only on the vertical displacement response of the Lysefjord Bridge, which is dominated by only few modes at frequencies below 1 Hz. Since the vehicle response is not studied here, a moving mass model[53] is found adequate to investigate the vehicle-induced bridge response. The use of a moving mass model is also supported by the fact that the high-frequency range of the bridge displacement response is negligible compared to its low-frequency response. A preliminary analysis using a more detailed moving oscillator model led to an almost identical bridge displacement response as the moving mass model, which was, therefore, chosen.

Since the wind load affects the total damping of the bridge, the identification of the vehicle characteristics needs to be conducted with a mean wind speed as low as possible. The mean wind speed is denoted hereafter as $\bar{u}$ where the overbar denotes the temporal average, as used in micrometeorology.[54] In the following, only bridge acceleration records associated with a mean wind speed below 5 m s^{-1} and a turbulence intensity lower than 15% are selected. Non-stationary wind fluctuations are commonly observed at such wind velocities. The first-order stationarity of each 30-min-long time series is tested using a moving mean with a centered half window of 5 min. Samples showing a moving mean value deviating by more than 20% of the static mean fail the stationary test and are thus disregarded. The remaining samples are found to have a negligible contribution to the bridge response compared to traffic loading.

The bridge vibration records associated with the selected velocity records are then used to identify if and when a vehicle crosses the bridge. This is achieved in four steps, as shown in Figure 3, and listed as follows:

a. The vertical acceleration response at midspan is transformed into the displacement response to amplify the influence of the low-frequency bridge response on its total motion. For that purpose, the discrete Fourier transform was used as it generally provides more accurate results.[55] In the present case, however, the double integration method could also be used as the focus is on the low-frequency range of the bridge response.
b. To isolate the background response of the bridge deck from its resonant response, zero-phase digital low-pass and high-pass fifth-order Butterworth filters are successively applied. The direct application of a band-pass filter may lead to an unstable output for the range of frequencies considered, which justifies the use of these two filters. The

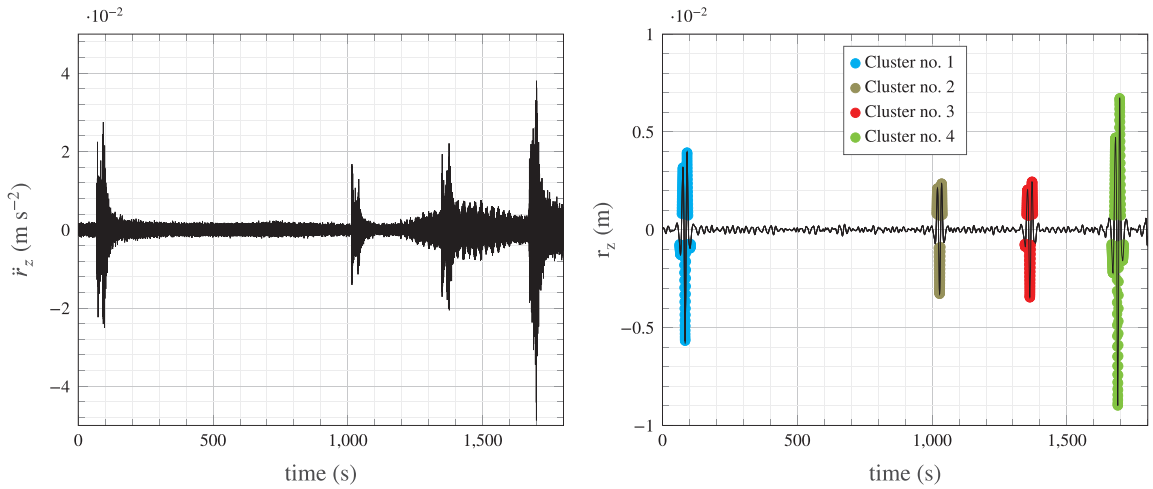

FIGURE 3 Acceleration data (left) and associated filtered bridge displacement response at midspan (right) recorded on September 9, 2017, at midnight, with four clusters identified at around $t = 83$ s, $t = 1{,}028$ s, $t = 1{,}361$ s, and $t = 1{,}788$ s

cut-off frequency for the high-pass filter is set to 0.04 Hz. This limit is fixed by the accelerometers' performances and the record duration as measurement errors in the acceleration data gradually increase when the frequency decreases.[23] The cut-off frequency for the low-pass filter is 0.15 Hz. This value is lower than the first vertical eigenfrequency, which is equal to 0.22 Hz. The use of fifth-order filter not only does allow for a stable filter design but also helps to enhance the displacement of the bridge due to traffic with respect to other sources of vibrations. To magnify even more the background response compared to the resonant response, a fourth-order filter or even third-order filter may be reliably applied. For the sake of brevity, the study of the optimal filter order is not considered in the following, and only the fifth-order filter is used.

c. To have a first estimate of the time at which a vehicle crosses the bridge, the transient bridge response associated with the passage of vehicles is extracted from the ambient response. This is achieved using an outlier analysis, based on the generalized extreme Studentized deviate test for outliers.[56] Note that a moving-median filter can also be applied to detect when vehicles cross the bridge. In this case, a higher number of outliers are detected. The detection of outliers using the moving median seems to perform best when a high number of lightweight and heavy vehicles cross the bridge. This method is, however, more sensitive to false-positive results and is, therefore, not considered in the following.
d. To associate each group of outliers to a vehicle, a clustering algorithm is applied. A clustering analysis aims to partition scattered data into groups. For a single group, the data share the same properties; that is, they are homogeneous, whereas, for multiple groups, a strong heterogeneity is visible. As the number of vehicles are a priori unknown, a hierarchical cluster tree is first built using the single linkage algorithm using Euclidian distance. Here, the term "Euclidian distance" has actually the dimension of time as two outliers are considered in the same cluster if they are separated by less than 30 s. This corresponds to the duration to cross the bridge main span (446 m) at a speed slightly above 50 km h^{-1}. In the present case, up to nine clusters per 30-min records are detected. Clusters recorded at the very beginning or at the end of the time series are also dismissed as they do not allow a reliable estimation of the arrival time and departure time of the vehicle crossing the bridge.

Clusters separated by less than 90 s are dismissed as they are assumed to correspond to vehicles that are too close to each other to be properly identified. This is, for example, the case if two vehicles of similar weight and speed are on the bridge at the same time. If one of the vehicles is significantly heavier than the other one, the selected cluster corresponds mainly to the bridge response associated with the passage of the heavier vehicle. The duration of 90 s is arbitrarily chosen for the case at hand and facilitates the selection of high-quality transient bridge response events. Nevertheless, the probability that one cluster corresponding to two vehicles of similar mass is selected is not 0. In this case, the root-mean-square error (RMSE) between the computed and measured response will be unusually large since a single moving mass model is used for identification purpose. The use of multiple moving mass is not considered hereafter as the number of uncertainties would considerably increase, unless surveillance cameras or other sensors are deployed to capture the arrival time and departure time of each vehicle.

Once each cluster is identified, the filtered displacement histories are cut into several segments, each of them centered around one cluster. The median value of the time for each cluster corresponds to a first guess for the vehicle arrival time. Each segment is associated with the quasistatic vertical response of the bridge to a single vehicle. According to the moving mass model, each vehicle is characterized by only two parameters: a horizontal speed and a mass. To facilitate their identification, the bridge displacement response in each segment is divided by its maximal absolute value. This normalization minimizes the dependency of the response on the vehicle mass. For the sake of simplicity, only the average vehicle speed is considered, although the vehicle speed is generally lower when the vehicles enter the bridge from the north than when they enter from the south.

For each segment, the normalized bridge response can, therefore, be characterized in terms of vehicle arrival time and vehicle speed. The arrival time is defined here as the time at which the bridge response due to traffic loading is detected by the accelerometers at midspan and corresponds to the time at which a vehicle arrives on either the north side or the south side of the bridge's main span. For each cluster, these two parameters are simultaneously estimated by minimizing the RMSE value between the computed and recorded vertical response of the bridge deck at midspan. This implies that each vehicle is detected independently from each other. As shown in Figure 4, the surface response of the RMSE value is computed for each cluster and is only a function of the arrival time and vehicle speed. At midspan, the surface response displays only one minimum, which is a global minimum. The global minimum is, therefore, searched iteratively, and convergence is assumed achieved when the changes in the value of the estimated vehicle speed and arrival time are below 0.5 km h^{-1} and 0.5 s, respectively.

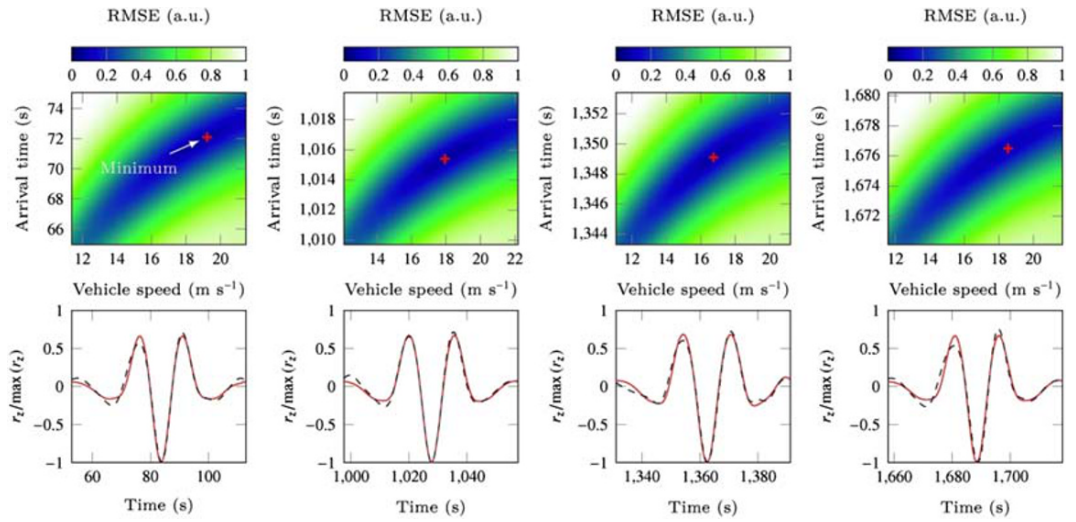

FIGURE 4 Top panel: root-mean-square error (RMSE) between the computed and measured quasi-static displacement response for the four clusters identified and displayed in Figure 3. Bottom panels: measured (– – – –) filtered displacement response superposed to the computed one (——) after estimating the vehicle speed and arrival time

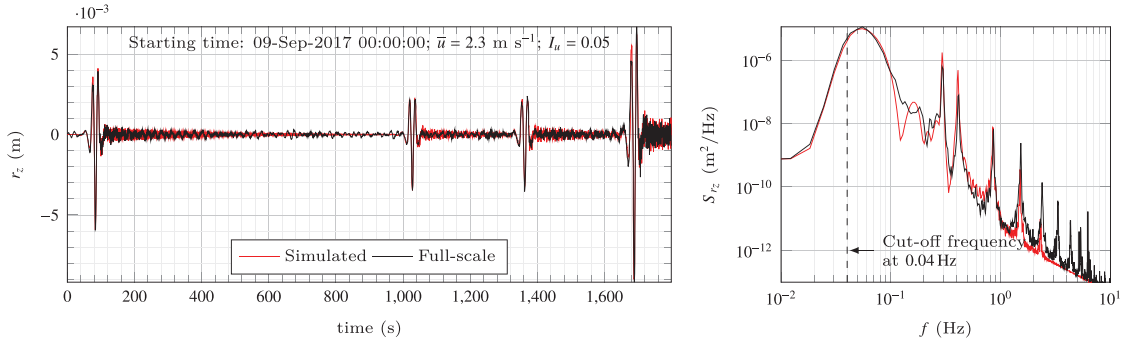

FIGURE 5 Time series (left panel) and associated power spectral density estimate at midspan (right panel) corresponding to the high-pass-filtered vertical bridge displacement response induced by the crossing of four vehicles, the parameters of which (arrival time, mass, and average speed) have been automatically estimated using the quasi-static response

As the bridge computational model is symmetric, the direction of a single moving vehicle has no influence on the displacement response at midspan. In full-scale, neglecting the vehicle direction is an acceptable approximation only if the acceleration records are collected at midspan. Once the vehicle average speed and arrival time are known, the vehicle mass is estimated in the least-squares sense using the non-normalized bridge displacement response and a moving mass model.

With a moving mass model, each vehicle is defined by only three parameters: arrival time, equivalent mass, and equivalent traveling speed. The adjective "equivalent" used here refers to the mass and speed estimated by the moving mass model at a constant speed that produces a computed response similar as observed in full-scale, even though the real mass and speed of the vehicle may be slightly different. For example, using the study case of Fadnes,[57] who observed a single 50-t truck crossing the Lysefjord Bridge moving at an average speed of 45 km h^{-1}, the computational model results in an equivalent mass of 58 t and a speed of 50 km h^{-1} for for a first crossing and a mass of 45 t and a speed of 56 km h^{-1} for a second crossing, 2 h later. The truck mass was not precisely known, its speed was not constant, and its loading was likely different during the two trips. Nevertheless, the estimated parameters are consistent with those from the full-scale observations and lead to a good agreement between the computed and measured bridge displacement response.

The applicability of the moving mass model is illustrated in Figure 5, where the computed and the full-scale high-pass-filtered bridge displacement response at midspan are superposed. In this figure, the bridge response is computed based on the parameters identified in Figures 3 and 4, for the four vehicles crossing the bridge. The remarkably good agreement between the two power spectral density estimates shows that for the wind conditions considered, the

turbulent wind load is of secondary importance and that the parameters used with the data post-processing are appropriate. Note that in the right panel of Figure 5, the peak recorded below 0.1 Hz is narrower than the spectra of the complete quasi-static vertical bridge response, due to the application of the high-frequency filter. The frequency at which this peak occurs corresponds roughly to the inverse of the time a vehicle needs to cross the main span of the bridge.

2.3 | Application to structural damping estimation

The structural damping is usually estimated by accounting for the aerodynamic damping component defined through the quasi-steady theory for turbulent wind loading at different reduced velocities. When doing so, the stationarity requirement for the wind excitation records is not always mentioned or fully investigated. As already pointed out,[58,59] a non-stationary input signal introduces additional uncertainties and, in general, an overestimation of the damping ratios.[59]

The methodology used here to obtain damping values relies on traffic-induced displacement decays, similarly to Rainer and Van Selst,[33] where a controlled vehicle impact was used as an excitation source for all the modes. Assuming that the vibration modes are sufficiently separated so that the resonant response for each eigenfrequency can be isolated, the damping ratio for each mode is estimated by the least-squares fitting of an SDOF system response to the monitored modal displacement free decay. The low traffic density generally recorded at the Lysefjord Bridge and the regular occurrence of heavy vehicles represent the opportunity to develop the aforementioned automated system identification approach. The structural damping can, therefore, be studied without performing forced resonance tests, which are challenging for long-span bridges.[60] Hence, the method is intended to be complementary to the modal identification techniques previously applied using data from the Lysefjord Bridge.[36,40,41]

The procedure detailed hereafter aims to estimate the damping ratios using traffic as the excitation source. The main idea is to search for the decay signals for each mode of the structure and estimate the corresponding damping, provided that no other vehicles are crossing the bridge and no vehicle enters the bridge for the duration of the analyzed decay. Traffic excitation is, therefore, used here in the same way as an impulse load or an imposed displacement is adopted in free vibration tests.[35] The identification of the vehicle characteristics becomes thus essential, and the knowledge of the vehicles' crossing time is necessary to study the onset of traffic-induced decays. To estimate the damping ratios, the automatic vehicle identification algorithm is followed by few additional steps: once a vehicle departure time is identified, which corresponds to the onset of the displacement decay, the modal displacements are computed via time-domain decomposition (TDD).[61] Then, an exponentially damped cosine function is fitted to each corresponding decay signal to obtain an estimate of the damping and eigenfrequency.

The automatic identification procedure is applied to the bridge vertical acceleration response at midspan. While in Section 2.2, clusters with a separation of 90 s or higher were used, the separation required to estimate the damping ratios needs to be at least 300 s to avoid overlapping of the free decays. This separation is crucial for the lower modes, which have a period of vibration up to 7.6 s. Based on the records collected between July 2017 and June 2018, 1,284 vehicles are automatically detected. An example of the identified arrival time and departure time is depicted in Figure 6.

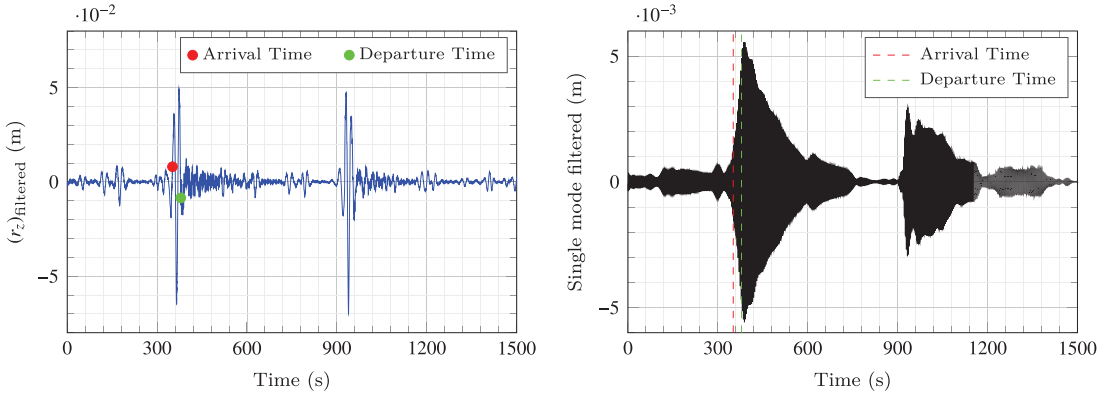

FIGURE 6 Example of arrival time and departure time from the traffic-induced vibrations characterisation: high-pass-filtered displacement at midspan (left panel); single-mode VS1 filtered displacement at midpsan (right panel)

2.3.1 | TDD and least-squares fit of the free-decay response

The time-domain decomposition (TDD) is an output-only modal analysis technique based on the multi-output response of a linear structural dynamic system.[61] This method is used here to retrieve the modal displacement response of the Lysefjord Bridge using all four pairs of accelerometers as input signal sources. This bridge exhibits well-separated modes; namely, the dynamic response of the system in the vicinity of each resonance condition is dominated by one mode only. Hence, TDD is applicable. Starting from acceleration time histories acquired by the sensors, modes are isolated using band-pass filtering and transformed into modal displacement $\eta_i(t), i=\{y,z,\theta\}$.[61] The implemented TDD is able to enhance the quality of the data and the subsequent damping estimation. In fact, low signal-to-noise ratios tend to broaden the energy of the spectral peaks, and therefore, the free-decay tails would artificially alter the damping estimation.

In the present work, the linear viscous damping model is adopted, assuming that it represents well the different energy dissipation mechanisms involved in the structural system. The free-decay response of an SDOF lightly damped system can be computed as follows:

$$d(t) = A\ddot{m}e^{-\omega_n \xi t}\cos(\omega_D t + \phi), \tag{1}$$

where $d(t)$ is the target decay signal, starting at peak amplitude A; ω_n is the circular eigenfrequency; ξ is the damping ratio; $\omega_D = \omega_n\sqrt{1-\xi^2}$ is the damped eigenfrequency; ϕ is the phase; and t is the time. This exponentially damped cosine function is fitted to the free-decay signals described above. It has been observed that for the torsional and horizontal modes, the so-called build-up (increasing amplitudes) starts as the vehicle enters the bridge and the peak of the single mode-filtered signal generally occurs at the departure time, whereas vertical modal displacement peaks are usually shifted two to three cycles from the departing time. For each mode, it is important to trace the exact time instant when the transient increasing amplitude response induced by the sudden change in the loading conditions becomes negligible with respect to the free oscillations. The entire fitting procedure is further challenged by the "beating" phenomena, which can arise within the decay due to the wind buffeting and/or the potential presence of light vehicles undetected by the identification algorithm. Decay signals, which exhibit substantial beating, are dismissed before the fitting process, and an additional quantitative control based on the RMSE of the fitting is applied in the post-processing phase.

The decay signal envelopes can be obtained using either the Hilbert transform or the local maxima within each period of the signal. The latter technique is adopted here to avoid the end effects in the Hilbert transform, which may influence the fitting process and the corresponding RMSE value.

The outcome of the fitting procedure depends on the number of cycles considered within the decay signal. The number of cycles were chosen as a reference parameter since it allows a consistent comparison of the identified damping ratios for the different modes. When selecting the number of cycles for each mode, a trade-off should be made between the necessity to capture the fully developed decay and the possibility to encounter potential noisy tails. To detect the presence of amplitude-dependent damping ratios, the damping is estimated using a moving rectangular window without overlapping. The absolute maximum within the decay is selected as representative amplitude value, and Equation (1) is fitted to the windowed normalized modal displacement decay, providing (1) damping ratio ξ, (2) undamped eigenfrequency ω_n, and (3) RMSE, as shown in Figure 7.

3 | ASSESSMENT OF TRAFFIC LOADING AND DYNAMIC RESPONSE

3.1 | Automatic identification of vehicles

The identification procedure illustrated in Figures 3 to 5 is repeated for each 30-min acceleration record at midspan between July 2017 and June 2018. The ability of the aforementioned algorithm to capture and model traffic-induced vibrations under low wind speed conditions is demonstrated in Figure 8, where the computed bridge response is compared to the one estimated from the full-scale measurements. The bridge response is herein studied in terms of the standard deviation and maxima of the dynamic vertical displacement response at midspan, that is, by accounting for the resonant and the quasi-static frequency ranges. We remind that the load applied on the bridge is computed using a moving mass model and assumed to be entirely due to traffic since for the wind conditions considered, the wind load is

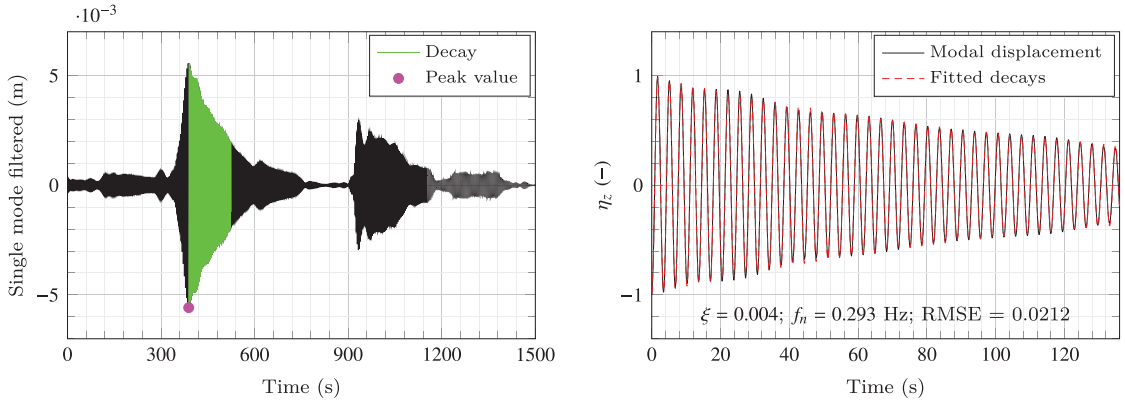

FIGURE 7 Example of filtered VS1 mode displacement response (left panel), with one window and 40 cycles and corresponding fitted SDOF system (right panel)

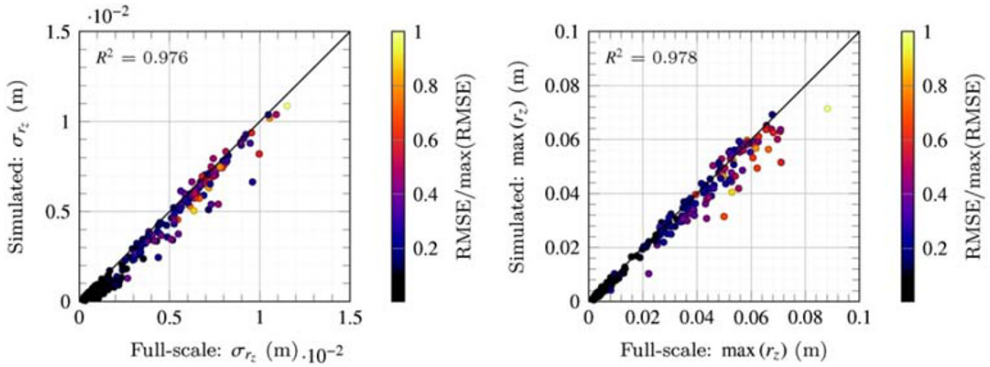

FIGURE 8 Computed and estimated standard deviation (left panel) and maximal value (right panel) of the displacement response of the Lysefjord Bridge at midspan for each times series where at least one vehicle is successfully identified (245 samples of 30-min duration)

found negligible. The samples considered here are only those where the traffic density is low, but at least one vehicle is identified. For each detected vehicle, the RMSE between the computed and estimated displacement response quantifies the reliability of the estimated vehicle mass and speed, leading to a distribution of RMSE values. The 95th-percentile value of the RMSE is used to filter out vehicles that have not been successfully identified by the algorithm. A large RMSE may be due to a low signal-to-noise ratio or indicate that the outlier detection algorithm or the cluster analysis failed to detect multiple vehicles crossing the bridge close together.

Figure 8 shows a good agreement between the computed and measured displacement response at midspan, in terms of the peak amplitude and standard deviation values. However, the discrepancies increase slightly with increasing vibration amplitudes. For $\sigma_{r_z} < 0.05$ m, the slight underestimation of the standard deviation of the simulated displacement response shown in the left panel of Figure 8 is expected, first because wind-induced vibrations are not modeled and, second, because we do not attempt to capture every vehicle crossing the bridge. This is especially the case when a mixture of multiple heavy and lightweight vehicles are recorded in a short period, such that the outlier detection algorithm ignores the lighter ones. This particular issue can be solved using an outlier detection algorithm relying on a local median, as described in Section 2.2.

The distribution of identified vehicle equivalent mass and speed is displayed in Figure 9. The term "distribution" refers here to the joint distribution of mass and speed responsible for a bridge response large enough to be detected by the outlier algorithm. In particular, the number of detected lightweight vehicles crossing the bridge at a low speed may be substantially lower than in reality as they produce a lower bridge response than heavyweight vehicles moving at a high speed. Nevertheless, the range of vehicle speeds is plausible and consistent with those documented by Fadnes[57] on March 7, 2017, although the lack of monitoring data from this day prevents a more detailed comparison.

Using a single pair of accelerometers at midspan to model the vehicle-induced response has the major advantage to require no knowledge of each vehicle direction since the bridge model is symmetrical. However, if the four pairs of accelerometers are simultaneously used, a poor fit of the quasi-static response can be obtained if the direction of each vehicle is not modeled.

In the present case, the most reliable way to account for the direction of the vehicles is to assume first that each of them comes from the north side of the bridge. If the computed quasi-static bridge response to a vehicle is obtained with

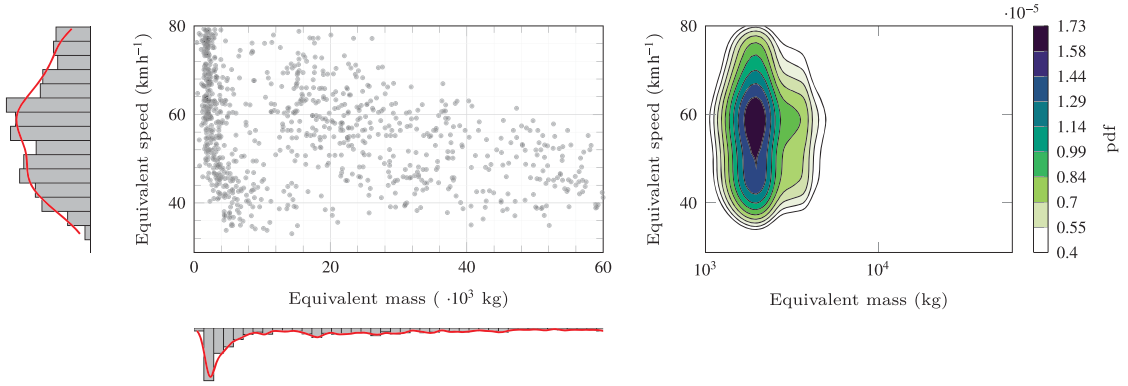

FIGURE 9 Distribution of the equivalent mass and speed of each identified vehicle crossing the Lysefjord Bridge and the associated kernel density estimate (left), which are combined into a joint-probability distribution (right)

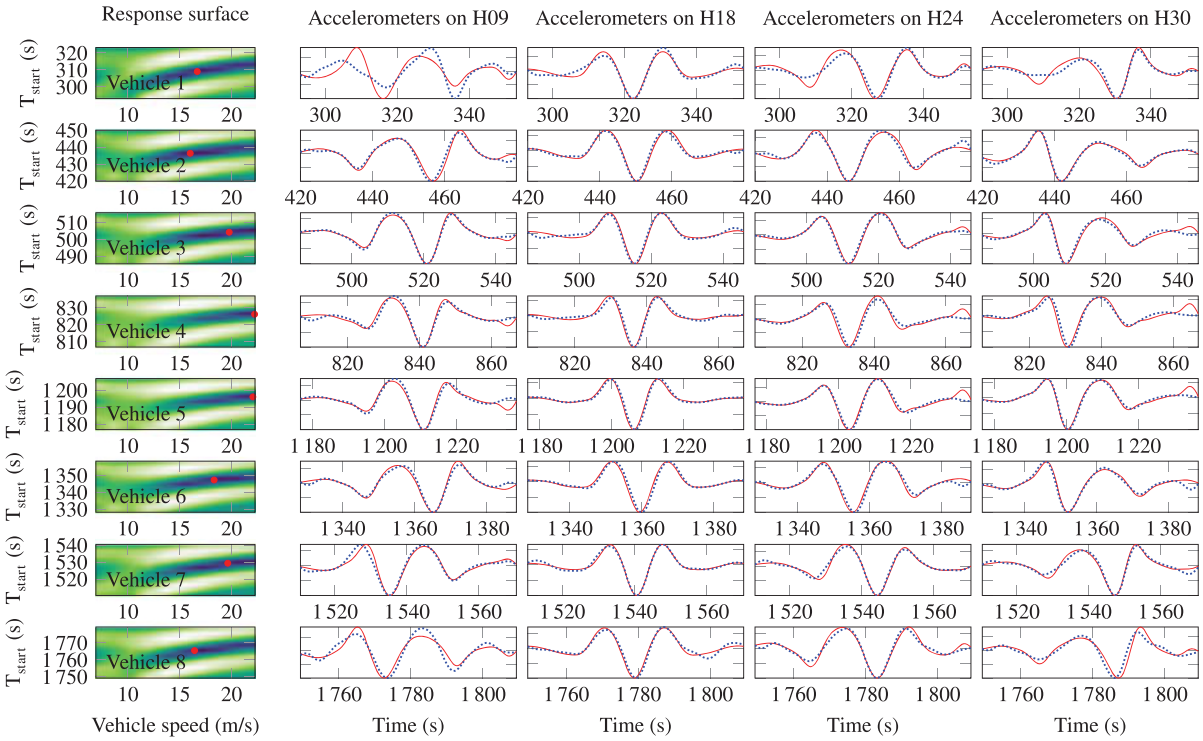

FIGURE 10 Fitted (——) and measured (– – – –) normalized quasi-static vertical response of the deck using the four pairs of accelerometers on January 7, 2017, from 04:30 to 05:00 during which eight vehicles were identified

a large root-mean-square error, this indicates that the vehicle comes likely from the southern side. In this situation, a new fitting is applied by changing the direction of the moving mass. In most cases, a reduction of the RMSE value by a factor 3 to 6 is observed, implying that the vehicle direction has been properly accounted for. Figure 10 illustrates the adequacy of the fitting procedure using a single 30-min record on July 1, 2017, from 04:30, during which eight vehicles were detected. In Figure 10, the response surfaces and the normalized quasi-static vertical displacements near H09, H18, H20, and H30 are calculated as in Figure 4. The red dot in each surface response corresponds to the global minimum for which the arrival time and equivalent speeds are identified. In Figure 10, the Vehicles 3, 4, 5, and 6 were found to come from the southern side and were thus identified after the application of a second fitting.

Using the entire data set from July 2017 to June 2018 and the four pairs of accelerometers, the standard deviation and maximal value of the computed and measured dynamic bridge response to the passage of vehicles are compared in Figure 11. The application of multiple synchronized accelerometers increases slightly the number of vehicles successfully identified but does not significantly improve the agreement between the computed and measured bridge response.

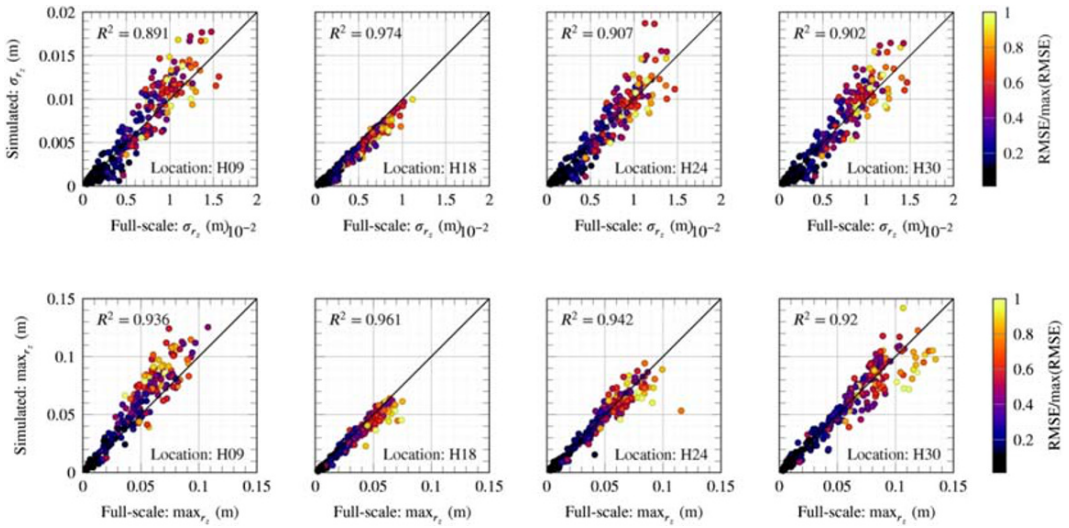

FIGURE 11 Computed and estimated standard deviation (top panels) and maximal value (bottom panels) of the displacement response of the Lysefjord Bridge from each pair of accelerometers, at H08, H18, H24, and H30 (310 samples of 30-min duration)

The best agreement is found near H18, which supports the application of a single measurement location, at midspan, as a cost-effective solution. The correlation coefficients are found to slightly decrease further from midspan. The measurement suggests that this is partly due to the underestimation of the structural damping by the computational model near the ends of the bridge after the vehicle leaves the main span. This could be due to the dependency of the damping on the amplitude of the vibrations, larger structural damping near the towers, or the variation of the speed of vehicles, which is not modeled here.

3.2 | Combined effect of wind and traffic loading

To evaluate the significance of traffic loading with respect to wind loading, the present section investigates their combined effects on the bridge response in the time domain. The bridge model is the same as in Section 2.2. The turbulent wind load is modeled using the Norwegian guideline for suspension bridge design.[62] The turbulence intensities at deck height for the along-wind and vertical velocity components are I_u=0.15 and I_w=0.7I_u, respectively. These turbulence intensity values are representative of the wind conditions from south to southwest at the bridge site.[63] For $i = \{u,w\}$, the one-point velocity spectrum is modeled as follows:

$$\frac{fS_i}{\sigma_i^2} = \frac{A_i n_i}{(1+1.5A_i n_i)^{5/3}}, n_i = \frac{fL_i^x}{\bar{u}(z)}, \tag{2}$$

where A_u=6.8, A_w=9.4, and L_i ($i = \{u,w\}$) is the integral length scale, defined as follows:

$$L_u^x = \begin{pmatrix} L_1(z/z_1)^{0.3}, & \text{if } z > z_{\min}, \\ L_1(z_{\min}/z_1)^{0.3}, & \text{if } 0 \le z \le z_{\min}, \end{pmatrix} \tag{3}$$

$$L_w^x = L_u^x/12, \tag{4}$$

where L_1 is a reference length scale equal to 100 m and z_1 is a reference height equal to 10 m, as prescribed in the Eurocode.[64] Finally, the lateral coherence is modeled using the Davenport model[65] with the decay coefficients $c_u^y = 10$ and $c_w^y = 6.5$ for the along-wind and vertical wind components, respectively. The stationary turbulent wind field is generated in the time domain using the traditional spectral representation approach.[66] The wind-induced response of the

bridge is computed in the time domain using the quasi-steady theory, in a similar fashion as by Wang et al., [47] except that the simpler continuum bridge model is used instead of the more detailed finite element model.

The combined effects of wind and traffic loading on the bridge response are here briefly assessed using three situations: (1) the case of a single 10-t vehicle crossing the bridge one time at a speed of 50 km h^{-1}; (2) the case of a single 40-t vehicle crossing the bridge one time at a speed of 45 km h^{-1}; and (3) the case of multiple vehicles crossing the bridge at different speed and time, as observed on February 23, 2018, between 12:00 and 12:30. For the latter case, the identified arrival time, equivalent mass, and speed of the vehicles are summarized in Table 1. For the three situations considered, both the traffic and wind loads are simultaneously accounted for. To assess the relative importance of these two sources of vibrations, the computation of the bridge response is repeated for the same traffic loading but with increasing mean wind speed and thus an increasing dynamic wind load (Equations 2 and 3).

For the three situations considered, Figure 12 shows that the standard deviation of the bridge displacement response is systematically underestimated if traffic is neglected. While the load induced by the 10-t vehicle contributes little to the standard deviation of the vertical bridge displacement response, the contribution of the single 40-t vehicle is not negligible, unless the mean wind speed $\bar{u}$ is larger than 14 m s^{-1}. In the case of multiple vehicles crossing the bridge, traffic is the dominant source of vibrations at $\bar{u} \leq 10$ m s^{-1}, and its contribution remains above 10% of the vertical displacement response up to $\bar{u} = 18$ m s^{-1}. The results displayed in Figure 12 are consistent with those from Macdonald,[67] who noted that traffic loading on the Second Severn Crossing Bridge, which has similar dimensions as the Lysefjord Bridge, was dominant at mean wind speed below 12 m s^{-1}.

Figure 12 brings additional proof that the study of the buffeting response of a suspension bridge in full-scale needs to account for traffic loading. Nevertheless, the results displayed in Figure 12 depend on the bridge structure considered and on the turbulence model used. In particular, increased turbulence intensity will reduce the influence of the traffic loading on the bridge response with respect to wind loading.

The comparison between the low-frequency and high-frequency ranges of the acceleration bridge response can also be used as a simple test to evaluate whether wind or traffic is the dominating source of vibration.[46] Using the vertical response of the Lysefjord Bridge at midspan, the first three symmetric vertical modes are assumed to belong to the low-frequency range while the higher vertical modes belong to the high-frequency ranges. Therefore, the limit between these two frequency ranges is set at f_t=1Hz. The ratio between the standard deviation of the response due to the high-frequency and the one at low-frequency is denoted $Q_{\hat{\dot{a}}_z}$:

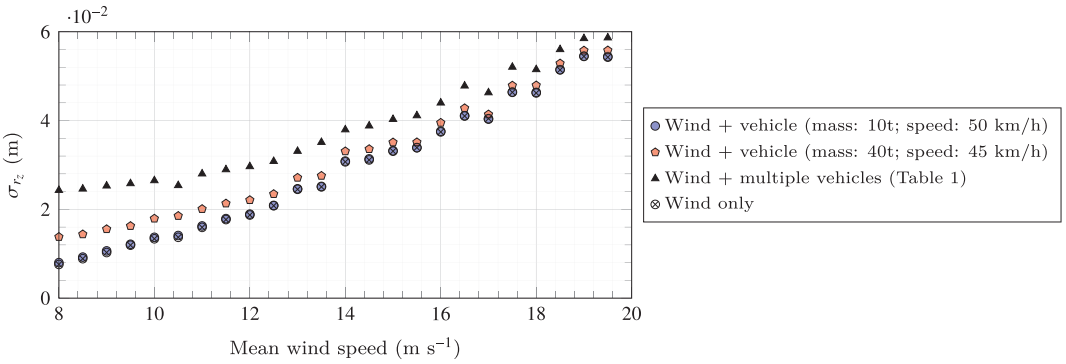

FIGURE 12 Standard deviation of the computed vertical bridge displacement response at midspan induced by wind turbulence and/or a single vehicle crossing the main span

TABLE 1 Vehicle parameters used in Figure 12 for the case "wind + multiple vehicles"

Vehicle number	1	2	3	4	5	6	7
Arrival time (min)	12:02:39	12:08:04	12:12:26	12:20:04	12:21:54	12:25:02	12:28:46
Equivalent mass (t)	15.5	51.8	56.7	24.2	17.0	15.5	26.4
Equivalent speed (km h^{-1})	66	53	49	61	66	66	57

[a]*Note.* The vehicle parameters are estimated from a 30-min acceleration records obtained on February 23, 2018, from 12:00, which was characterized by multiple heavy-weight vehicles crossing the bridge in less than 30 min.

$$Q_{\hat{A}_z} = \frac{\sqrt{\int_{f_t}^{f_c} S_{\hat{A}_z}(f)\, df}}{\sqrt{\int_{f_0}^{f_t} S_{\hat{A}_z}(f)\, df}} \tag{5}$$

where f_0 is the lowest frequency recorded and f_c is the Nyquist frequency. If $Q_{\hat{A}_z} > 1$, the bridge response is dominated by traffic loading. Otherwise, the wind load is the dominant source of excitation. Using this method, traffic was observed to be the main source of vibrations in most of the cases at wind speed below 10m s^{-1} in Cheynet.[46]

Figure 13 shows that the signature of traffic-induced vibrations is clearly visible in the PSD of the bridge acceleration response. For the sake of clarity, the frequency-domain decomposition[25] has been applied to extract the first singular value of the cross-spectral density matrix, which contains both the symmetric and asymmetric modes. The first singular values are then normalized by their maxima to ensure a consistent comparison between the cases selected. The two samples considered are recorded on January 23, 2018, from 00:00 to 10:00 with a fairly stationary mean wind speed of 5 m s^{-1}. From 00:00 to 05:00, little traffic is recorded, and wind loading is the dominating source of vibrations. From 05:00 to 10:00, traffic loading predominates over wind loading. Therefore, $Q_{\hat{A}_z} > 1$ for the case where traffic is dominating (red curve) while $Q_{\hat{A}_z} < 1$ when wind loading is dominating (black curve). The signature of traffic loading is clearly visible at frequencies above 1 Hz and at low frequencies, between 0.01 and 0.1 Hz, where a clear bump is visible. This bump, which is also highlighted in Figure 5 for the displacement response, shows the quasi-static vertical response of the bridge to passing vehicles. It is the key feature captured by the algorithm described in Section 2.2.

4 | DAMPING RATIO IDENTIFIED FROM TRAFFIC-INDUCED RESPONSE

The damping estimates of the Lysefjord Bridge are computed based on the free-decay response as described in Section 2.3. A single-window of 40 cycles is adopted for the damping estimation, as it provides a good trade-off between decay fitting quality, minimization of standard deviation, and number of reliable outcomes. To reduce the influence of outliers on the statistical representation of the damping and enhance the quality of the analyzed signals, we focus on values below the 95th percentile only. The identified eigenfrequencies are corrected for the effect of temperature, assuming a negative linear relationship between the eigenfrequencies and temperature.[68-70]

To assess the quality of the modal parameter estimates based on traffic-induced decays, an automated SSI-COV algorithm inspired by Magalhaes et al.[44] and Magalhães and Cunha[71] is applied to the 30-min-long acceleration signals mentioned in Section 2.3. The adopted time lags τ for the correlation functions correspond here to three or four times the largest eigenperiods, as used by Brownjohn et al.[39] and Magalhaes et al.[44]. Damping and eigenfrequency estimates are hereafter presented using the quantity $\tilde{k} \pm \sigma_k$ (where k=ξ,f_n), which stands for median value ± standard deviation.

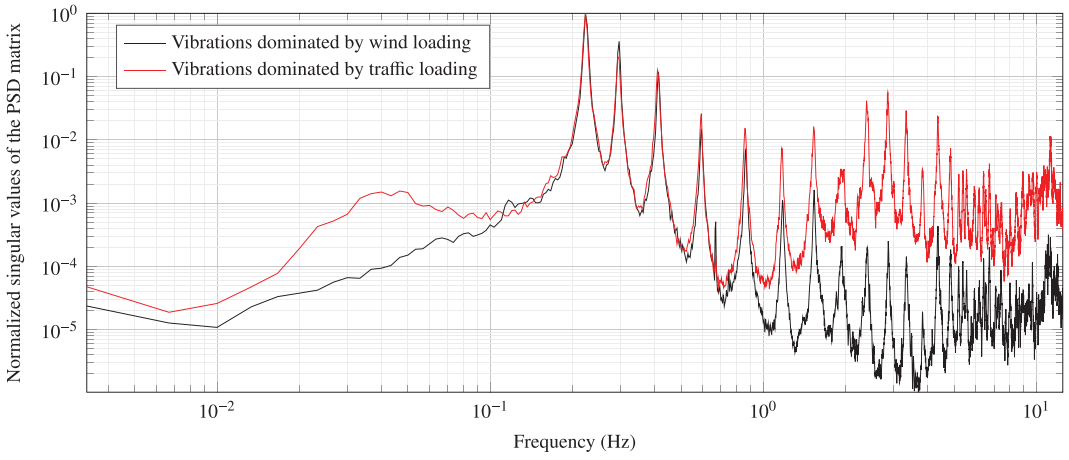

FIGURE 13 Normalized singular values of the cross-spectral density matrix of the vertical bridge acceleration recorded from January 23, 2018, from 00:00 to 05:00 (black curve) and from 05:00 to 10:00 (red curve) with $\bar{u}(z = 60\text{m}) \approx 5$ m s^{-1}

The computation of the aerodynamic damping based on the quasi-steady theory for wind loading is not applicable at low wind speed. To account for the dependence of the damping ratios on the mean wind speed, it is possible to establish an empirical relation based on a second-order polynomial fit. However, in the present study, it does not provide a clear relationship for all the modes considered. Nevertheless, the aerodynamic contribution in the estimated damping is found insignificant for mean wind speed below 5 m s^{-1}, and the damping ratios considered here are, therefore, assumed to be representative of the structural damping associated with each mode.

No clear relationship between the damping and bridge deck response was found for the modal displacement magnitudes involved in the free vibration records. However, a reduction of the eigenfrequencies with increasing traffic loading, highlighted by recent studies,[72-74] is expected. During the nighttime, both the traffic loading and the air temperature are lower, implying higher eigenfrequencies than during daytime. For the dataset considered, the relative change of the eigenfrequency is up to −1% for the mode VS1 and up to −2% for the mode HS1. However, in the case of the mode TS1, the eigenfrequency values do not show any clear reduction with increasing amplitude of bridge deck response.

The median value and the standard deviation of the estimated damping ratios, as well as the corresponding eigenfrequencies for all the considered modes, are reported in Table 2. The median damping estimates are in general agreement with full-scale observations on long-span bridges available in Simiu and Miyata,[75] and the corresponding standard deviations are lower than 0.22% for all the modes considered. Such a low scatter is achieved by automatically addressing high-quality single-mode decays with preidentified traffic loading cases. The estimated damping ratios for vertical and torsional modes are in the range $\xi \simeq$ 0.3–0.5%, which is expected for a steel welded box girder suspension bridge.[45] The damping of HS1 mode is 0.92%±0.22, which is in overall agreement with the median value 0.80% estimated in Cheynet et al.[36] using the automated SSI-COV algorithm and record durations of 1 h. The HS2 and HA2 modes, which are dominated by the motion of the main cables, exhibit low median damping values of 0.17% and 0.16%, respectively.

The median value and the dispersion of damping ratios estimated using the automated SSI-COV algorithm are, as expected, larger than the ones computed utilizing traffic-induced modal vibration decays (Table 2). Results based on ambient vibration tests usually show a rather high uncertainty level, mainly due to the finite length of records, the variation of the environmental conditions, and variability in the loading characteristics. Most of the median values obtained from traffic-induced vibrations lie within the range defined by median ± standard deviation of the damping ratios estimated using the automated SSI-COV algorithm, thereby validating in this way the goodness of the proposed methodology.

TABLE 2 Comparison between the traffic-induced decay method and the automated SSI-COV algorithm, showing the median value and standard deviation of the identified damping ratios ξ and un-damped eigenfrequencies f_n

	Traffic-induced decays				SSI-COV			
Mode	$\widetilde{f_n}$	σ_{f_n}	$\tilde{\xi}\ddot{n}10^{-2}$	$\sigma_\xi \cdot 10^{-2}$	$\widetilde{f_n}$	σ_{f_n}	$\tilde{\xi}\ddot{n}10^{-2}$	$\sigma_\xi \cdot 10^{-2}$
VS1	0.294	0.001	0.38	0.13	0.295	0.001	0.42	0.15
VS2	0.408	0.003	0.36	0.15	0.410	0.003	0.56	0.18
VS3	0.852	0.002	0.41	0.15	0.853	0.004	0.52	0.19
VA1	0.221	0.002	0.31	0.15	0.223	0.002	0.68	0.17
VA2	0.586	0.003	0.39	0.15	0.588	0.003	0.50	0.19
VA3	1.165	0.005	0.52	0.17	1.162	0.005	0.68	0.26
HS1	0.135	0.001	0.92	0.22	0.136	0.001	1.12	0.27
HS2	0.577	0.001	0.17	0.05	0.574	0.001	0.13	0.06
HS3	0.860	0.005	0.68	0.22	0.867	0.007	0.65	0.34
HA1	0.443	0.004	0.61	0.13	0.445	0.004	0.78	0.20
HA2	0.625	0.001	0.16	0.06	0.626	0.001	0.15	0.08
HA3	1.012	0.009	0.54	0.17	1.013	0.009	0.83	0.37
TS1	1.238	0.003	0.39	0.13	1.236	0.005	0.54	0.29
TS2	3.219	0.010	0.41	0.13	3.216	0.014	0.57	0.15
TA1	2.183	0.006	0.45	0.12	2.177	0.012	1.01	0.37

5 | CONCLUSIONS

We present an algorithm that automatically identifies the equivalent mass and speed of vehicles crossing a long-span suspension bridge utilizing ambient vibrations data. The first goal is to estimate vehicle characteristics that can be further used to gather information about the level of serviceability loading of the bridge, as well as provide relevant data for smart asset management. The second goal is to identify situations where the vehicle-induced response of the bridge can be exploited to estimate the bridge damping ratios using high-quality free-decay response.

The identification of the vehicles relies on the analysis of the background component of the vertical displacement response. First, traffic-induced vibrations are detected using an outlier detection algorithm and a cluster analysis. Then, a moving mass model is applied to estimate in the least-squares sense the time at which a vehicle arrives on the bridge as well as its average speed and mass. As the latter two parameters are estimated knowing the bridge response only, they are referred to as "equivalent mass" and "equivalent speed." Despite its simplicity, the use of a moving mass model is found adequate to describe the vehicle-induced bridge quasi-static and dynamic vertical displacement response. As the wind-induced vibrations are not modeled within the identification algorithm, it is primarily suitable for acceleration records associated with wind speed below 5 m s^{-1}. At present, the identification algorithm requires a low traffic density, as two vehicles crossing the bridge simultaneously or in a short time lead to two mixed-signal clusters that are not easily separated. As only vehicles inducing a noticeable bridge response are detected, the present algorithm is suitable to study vehicle-induced bridge vibrations rather than for traffic monitoring.

The simulation of combined traffic and wind loading on the Lysefjord Bridge shows that the dynamic response of the structure is in general underestimated if traffic loading is not accounted for. In some situations, as shown in Table 1, traffic loading can be a major source of excitation, even for a mean wind speed of 10 m s^{-1}.

Using the arrival time and departure time of the detected vehicles, the onset of traffic-induced displacement decay is studied for each vehicle. Once the free-decay response is identified, the time-domain decomposition algorithm is applied to retrieve the corresponding modal displacement. Then, the damping ratios and eigenfrequencies are estimated by fitting an exponentially damped cosine function to the decay signal. To minimize the impact of the aerodynamic damping on the estimated one, only free decays associated with stationary flow conditions and mean wind speed below 5 m s^{-1} were considered. It is found that the damping ratios of the low-frequency modes are estimated more accurately by this method than by the automated covariance-driven stochastic subspace identification algorithm. Therefore, the proposed procedure may be coupled with classical system identification techniques to study the damping ratios of a long-span bridge.

ACKNOWLEDGEMENT

The support of the Norwegian Public Roads Administration is gratefully acknowledged, as well as their assistance during the installation and maintenance of the monitoring system.

ORCID

Etienne Cheynet https://orcid.org/0000-0002-4854-1469
Jónas Snæbjörnsson https://orcid.org/0000-0003-4391-9925

REFERENCES

1. Farrar CR, James III GH. System identification from ambient vibration measurements on a bridge. *J Sound Vibr*. 1997;205(1):1-18.
2. Chan THT, Guo L, Li ZX. Finite element modelling for fatigue stress analysis of large suspension bridges. *J Sound Vibr*. 2003;261(3):443-464.
3. Chen SR, Cai CS. Equivalent wheel load approach for slender cable-stayed bridge fatigue assessment under traffic and wind: feasibility study. *J Bridge Eng*. 2007;12(6):755-764.
4. Chen ZW, Xu YL, Xia Y, Li Q, Wong KY. Fatigue analysis of long-span suspension bridges under multiple loading: case study. *Eng Struct*. 2011;33(12):3246-3256.
5. Chen SR, Wu J. Modeling stochastic live load for long-span bridge based on microscopic traffic flow simulation. *Comput Struct*. 2011;89(9-10):813-824.
6. Liu Y, Kong X, Cai CS, Wang Da. Driving effects of vehicle-induced vibration on long-span suspension bridges. *Struct Contrl Health Monit*. 2017;24(2):e1873.
7. Wang F-Y, Xu Y-L. Traffic load simulation for long-span suspension bridges. *J Bridge Eng*. 2019;24(5):5019005.
8. Yang Y-B, Lin CW, Yau JD. Extracting bridge frequencies from the dynamic response of a passing vehicle. *J Sound Vibration*. 2004;272(3-5):471-493.

9. Lin CW, Yang YB. Use of a passing vehicle to scan the fundamental bridge frequencies: an experimental verification. *Eng Struct*. 2005;27(13):1865-1878.
10. Yin X, Fang Z, Cai CS, Deng L. Non-stationary random vibration of bridges under vehicles with variable speed. *Eng Struct*. 2010;32(8): 2166-2174.
11. Malekjafarian A, OBrien EJ. On the use of a passing vehicle for the estimation of bridge mode shapes. *J Sound Vibr*. 2017;397:77-91.
12. Tan C, Uddin N, OBrien EJ, McGetrick PJ, Kim C-W. Extraction of bridge modal parameters using passing vehicle response. *J Eng*. 2019;24(9):4019087.
13. Yang YB, Zhang B, Chen Y, Qian Y, Wu Y. Bridge damping identification by vehicle scanning method. *Eng Struct*. 2019;183:637-645.
14. Li J, Zhu X, Law S, Samali B. Indirect bridge modal parameters identification with one stationary and one moving sensors and stochastic subspace identification. *J Sound Vibr*. 2019;446:1-21.
15. Chen SR, Cai CS. Accident assessment of vehicles on long-span bridges in windy environments. *J Wind Eng Indust Aerodyn*. 2004;92 (12):991-1024.
16. Chen SR, Wu J. Dynamic performance simulation of long-span bridge under combined loads of stochastic traffic and wind. *J Bridge Eng*. 2009;15(3):219-230.
17. Zhang W, Cai CS, Pan F. Fatigue reliability assessment for long-span bridges under combined dynamic loads from winds and vehicles. *J Bridge Eng*. 2012;18(8):735-747.
18. Xu Y-L, Guo WH. Dynamic analysis of coupled road vehicle and cable-stayed bridge systems under turbulent wind. *Eng Struct*. 2003;25 (4):473-486.
19. Cai CS, Chen SR. Framework of vehicle–bridge–wind dynamic analysis. *J Wind Eng Indust Aerodyn*. 2004;92(7-8):579-607.
20. Camara A, Kavrakov I, Nguyen K, Morgenthal G. Complete framework of wind–vehicle–bridge interaction with random road surfaces. *J Sound Vibration*. 2019;458:197–217.
21. Wang H, Mao J-X, Spencer Jr BF. A monitoring-based approach for evaluating dynamic responses of riding vehicle on long-span bridge under strong winds. *Eng Struct*. 2019;189:35-47.
22. Wong K-Y. Instrumentation and health monitoring of cable-supported bridges. *Struct Contrl Health Monit*. 2004;11(2):91-124.
23. Xu YL, Xia Y. *Structural Health Monitoring of Long-Span Suspension Bridges*. Boca Raton, FL: CRC Press; 2011.
24. Peeters B, De Roeck G. Reference-based stochastic subspace identification for output-only modal analysis. *Mech Syst Sig Process*. 1999;13 (6):855-878.
25. Brincker R, Ventura CE, Andersen P. Damping estimation by frequency domain decomposition. In: Proceedings of IMAC 19: A Conference on Structural Dynamics:February 5–8, Hyatt Orlando, Kissimmee, Florida, 2001 . Society for Experimental Mechanics. 2001: 698-703.
26. He XH, Hua XG, Chen ZQ, Huang FL. EMD-based random decrement technique for modal parameter identification of an existing railway bridge. *Eng Struct*. 2011;33(4):1348-1356.
27. Yu L, Chan THT. Recent research on identification of moving loads on bridges. *J Sound Vibration*. 2007;305(1-2):3-21.
28. Deng Lu, Cai CS. Identification of parameters of vehicles moving on bridges. *Eng Struct*. 2009;31(10):2474-2485.
29. Lalthlamuana R, Talukdar S. Estimation of gross weight, suspension stiffness and damping of a loaded truck from bridge measurements. *Struct Infrastruct Eng*. 2017;13(11):1497-1512.
30. Wang H, Nagayama T, Zhao B, Su D. Identification of moving vehicle parameters using bridge responses and estimated bridge pavement roughness. *Eng Struct*. 2017;153:57-70.
31. Bryja D, Śniady P. Random vibration of a suspension bridge due to highway traffic. *J Sound Vibration*. 1988;125(2):379-387.
32. BBC News. France bridge collapse: 50-tonne lorry "probably caused accident". accessed 2020-02-12. retrieved from https://www.bbc.com/news/world-europe-50479476; 2019.
33. Rainer JH, Van Selst A. Dynamic properties of Lions' Gate suspension bridge. In: ASCE/EMD Specialty Conference. University of California; 1976; Los Angeles:243-252.
34. Kareem A, Gurley K. Damping in structures: its evaluation and treatment of uncertainty. *J Wind Eng Indust Aerodyn*. 1996;59(2-3): 131-157.
35. Magalhães F, Cunha À, Caetano E, Brincker R. Damping estimation using free decays and ambient vibration tests. *Mech Syst Sig Process*. 2010;24(5):1274-1290.
36. Cheynet E, Jakobsen JB, Snæbjörnsson J. Damping estimation of large wind-sensitive structures. *Proc Eng*. 2017;199:2047-2053.
37. Bajrić A, Høgsberg J, Rüdinger F. Evaluation of damping estimates by automated operational modal analysis for offshore wind turbine tower vibrations. *Renew Energy*. 2018;116:153-163.
38. Jones NP, Spartz CA. Structural damping estimation for long-span bridges. *J Eng Mech*. 1990;116(11):2414-2433.
39. Brownjohn JMW, Magalhaes F, Caetano E, Cunha À. Ambient vibration re-testing and operational modal analysis of the Humber Bridge. *Eng Struct*. 2010;32(8):2003-2018.
40. Cheynet E, Jakobsen JB, Snæbjörnsson J. Buffeting response of a suspension bridge in complex terrain. *Eng Struct*. 2016;128:474-487.
41. Cheynet E, Snæbjörnsson J, Jakobsen JB. Temperature effects on the modal properties of a suspension bridge. *Dynamics of Civil Structures*, Vol.2. Cham, Switzerland: Springer; 2017:87-93.
42. Strømmen EN. Structural dynamics. *Structural Dynamics*. Cham: Springer International Publishing; 2014:89-159.
43. Sigbjörnsson R, Hjorth-Hansen E. Along-wind response of suspension bridges with special reference to stiffening by horizontal cables. *Eng Struct*. 1981;3(1):27-37.

44. Magalhaes F, Cunha À, Caetano E. Online automatic identification of the modal parameters of a long span arch bridge. *Mech Syst Signal Process*. 2009;23(2):316-329.
45. Larsen A, Larose GL. Dynamic wind effects on suspension and cable-stayed bridges. *J Sound Vibr*. 2015;334:2-28.
46. Cheynet E. Wind-induced vibrations of a suspension bridge: a case study in full-scale. *Ph.D. Thesis*: University of Stavanger, Norway; 2016.
47. Wang J, Cheynet E, Jakobsen JB, Snæbjörnsson J. Time-domain analysis of wind-induced response of a suspension bridge in comparison with the full-scale measurements. In: ASME 2017 36th International Conference on Ocean, Offshore and Arctic Engineering; 2017.
48. Luco JE, Turmo J. Linear vertical vibrations of suspension bridges: a review of continuum models and some new results. *Soil Dyn Earthq Eng*. 2010;30(9):769-781.
49. Fergestad D, Høyte J, Brathaug HP. Brukermanual til alvsat versjon 3.7: analyse av lineære svingninger av hengebru i vinduro; 1996.
50. Yang Y-B, Yau J-D. Vehicle–bridge interaction element for dynamic analysis. *J Struct Eng*. 1997;123(11):1512-1518.
51. Guo WH, Xu YL. Fully computerized approach to study cable-stayed bridge–vehicle interaction. *J Sound Vibration*. 2001;248(4):745-761.
52. Pan T-C, Li J. Dynamic vehicle element method for transient response of coupled vehicle-structure systems. *J Struct Eng*. 2002;128(2):214-223.
53. Jeffcott HH. VI. On the vibration of beams under the action of moving loads. *London, Edinburgh, and Dublin Philosophical Mag J Sci*. 1929;8(48):66-97.
54. Kaimal JC, Finnigan JJ. *Atmospheric Boundary Layer Flows: Their Structure and Measurement*: Oxford University Press; 1994.
55. Brandt A, Brincker R. Integrating time signals in frequency domain—comparison with time domain integration. *Measurement*. 2014;58:511-519.
56. Rosner B. Percentage points for a generalized ESD many-outlier procedure. *Technometrics*. 1983;25(2):165-172.
57. Fadnes TO. A full-scale study on traffic induced vibrations of a suspension bridge. *Master's Thesis*: University of Stavanger, Norway; 2017.
58. Brownjohn J. Estimation of damping in suspension bridges. *Proc Inst Civil Eng—Struct Buildings*. 1994;104:401-415.
59. Brownjohn JMW, Dumanoglu AA, Severn RT, Taylor CA. Ambient vibration measurements of the Humber suspension bridge and comparison with calculated characteristics. *Proc Inst Civil Engineers (London)*. 1987;83:561-600.
60. Cunha A, Caetano E, Delgado R. Dynamic tests on large cable-stayed bridge. *J Bridge Eng*. 2001;6(1):54-62.
61. Kim BH, Stubbs N, Park T. A new method to extract modal parameters using output-only responses. *J Sound Vibr*. 2005;282(1-2):215-230.
62. NPRA. *Bridge Projecting Handbook n400 (in Norwegian)*. Oslo, Norway: The Norwegian Public Roads Administration; 2015. https://doi.org/10.1115/OMAE2017-61725.
63. Cheynet E, Jakobsen JB, Snæbjörnsson J. Flow distortion recorded by sonic anemometers on a long-span bridge: towards a better modelling of the dynamic wind load in full-scale. *J Sound Vibr*. 2019;450:214-230.
64. EN 1991-1-4. Eurocode 1: actions on structures—part 1–4: general actions-wind actions; 2005.
65. Davenport AG. The spectrum of horizontal gustiness near the ground in high winds. *Quart J R Meteorol Soc*. 1961;87(372):194-211.
66. Shinozuka M, Deodatis G. Simulation of stochastic processes by spectral representation. *Appl Mech Rev*. 1991;44(4):191-204.
67. Macdonald JHG. Identification of the dynamic behaviour of a cable-stayed bridge from full scale testing during and after construction. *Ph.D. Thesis*: University of Bristol; 2000.
68. Xia Y, Chen B, Weng S, Ni Y-Q, Xu Y-L. Temperature effect on vibration properties of civil structures: a literature review and case studies. *J Civil Struct Health Monit*. 2012;2(1):29-46.
69. Li Z, Feng MQ, Luo L, Feng D, Xu X. Statistical analysis of modal parameters of a suspension bridge based on Bayesian spectral density approach and SHM data. *Mech Syst Signal Process*. 2018;98:352-367.
70. Zhou Y, Sun L. Effects of environmental and operational actions on the modal frequency variations of a sea-crossing bridge: a periodicity perspective. *Mech Syst Sig Process*. 2019;131:505-523.
71. Magalhães F, Cunha À. Explaining operational modal analysis with data from an arch bridge. *Mech Syst Sig Process*. 2011;25(5):1431-1450.
72. Koo K-Y, Brownjohn JMW, List DI, Cole R. Structural health monitoring of the Tamar suspension bridge. *Struct Contrl Health Monit*. 2013;20(4):609-625.
73. Westgate R, Koo K-Y, Brownjohn J. Effect of vehicular loading on suspension bridge dynamic properties. *Struct Infrastruct Eng*. 2015;11(2):129-144.
74. Mao J-X, Wang H, Feng D-M, Tao T-Y, Zheng W-Z. Investigation of dynamic properties of long-span cable-stayed bridges based on one-year monitoring data under normal operating condition. *Struct Contrl Health Monit*. 2018;25(5):e2146.
75. Simiu E, Miyata T. Design of buildings and bridges for wind: a practical guide for ASCE-7 standard users and designers of special structures; 2006.

How to cite this article: Cheynet E, Daniotti N, Jakobsen JB, Snæbjörnsson J. Improved long-span bridge modeling using data-driven identification of vehicle-induced vibrations. *Struct Control Health Monit*. 2020;27:e2574. https://doi.org/10.1002/stc.2574